Section VI. Materials Science

Amorphous Si – the role of MeV implantation in elucidating defect and thermodynamic properties *

J.M. Poate, S. Coffa [1], D.C. Jacobson and A. Polman

AT&T Bell Laboratories, Murray Hill, NJ 07974, USA

J.A. Roth and G.L. Olson

Hughes Research Laboratories, Malibu, CA 90265, USA

S. Roorda and W. Sinke

FOM Instituut voor Atoom- en Molecuulfysica, Kruislaan 407, 1098 SJ Amsterdam, The Netherlands

J.S. Custer and M.O. Thompson

Cornell University, Ithaca, NY 14853, USA

F. Spaepen and E. Donovan [2]

Harvard University, Cambridge, MA 02138, USA

The role of MeV implantation in producing thick amorphous Si layers has been central in elucidating several of its properties. The recent use of MeV Si beams to produce very pure layers will be reviewed. The kinetics of solid-phase epitaxy have been measured for amorphous Si layers up to 5 μm thick and the activation energy found to be 2.70 ± 0.02 eV. Calorimetry measurements of such thick layers show an interfacial heat release due to crystallization of 13.4 ± 0.7 kJ/mol and a homogeneous heat release of 5.1 ± 1.2 kJ/mol. This homogeneous heat release, associated with relaxation, is due to the annihilation of defects in the amorphous structure. These defects have been studied by ion-bombarding 500°C annealed amorphous and single-crystal Si. The formation and annihilation properties of the defects in these two states are intriguingly similar. Defects saturate in previously annealed a-Si at ion doses ~ 0.02 dpa. The presence of the defects is also manifested in measurements of the density of amorphous Si which is $(1.8 \pm 0.1)\%$ less dense than the crystal. The diffusion and solubilty of Cu, Zn, Pd, Ag, Pt and Au have been measured in amorphous Si and found to be very sensitive to defect population. The various experiments show that the intrinsic defect level in amorphous Si is 1–2 at.%

1. Introduction

Understanding the structure and properties of amorphous (a)-Si is a scientific challenge of some complexity [1]. Much progress has been made in the study of hydrogenated a-Si because of its technological importance. The study of a-Si formed by ion implantation has historically had very different driving forces. Interest has focussed on recrystallization phenomena because of the need to remove all damage and incorporate dopants on lattice sites. Important phenomena were discovered in these studies such as solid-phase epitaxy. This review will detail our recent experimental studies of the formation and properties of amorphous (a)-Si formed by MeV implantation. The question should be asked what special significance there is to producing micron thick amorphous layers by MeV beams rather than the thinner layers, typically 0.1 μm, produced in the usual low-energy implantation machines. The answer lies in the fact that the extra dimension permits better measurement of the following properties.

Four specific areas will be discussed:

(a) *kinetics* of solid-phase epitaxy of 5 μm thick layers where the behavior mimics that of much thinner layers but a novel ambient annealing effect has been observed,

---

(b) *calorimetry* studies of heat release of a-Si layers where the relaxation process has been identified in terms of defect annihilation,

(c) *density* measurements of a-Si where the role of defects are investigated, and finally

(d) *diffusion* studies where considerable progress has now been made in identifying diffusing species in a-Si and the role defects play in the diffusion mechanisms.

The a-Si layers described in these experiments were formed by [28]Si implantation using the National Electrostatics Corporation 1.7 MV tandem accelerator at AT& T Bell Laboratories.

2. Kinetics of solid-phase epitaxy

It is well established that a-Si layers formed by ion implantation into single-crystal (c) substrates can be crystallized epitaxially in the solid phase [2]. The kinetics of solid-phase epitaxy (SPE) have been extensively studied on amorphous layers less than 500 nm thick using time-resolved reflectivity (TRR) measurements [2], and it has been shown that SPE in these layers is characterized by an activation energy of 2.7 eV. The study of SPE in much thicker layers has recently become possible with the advent of MeV ion-implantation methods capable of producing high-purity a-Si films with thicknesses exceeding 5 μm. In order to monitor the location of the c/a interface during SPE and to accurately measure epitaxial growth rates in these layers, the TRR technique has been extended to infrared wavelengths where a-Si is nearly transparent, thus avoiding the thickness limitation imposed by absorption in the visible-wavelength region. In this way the SPE kinetics of very thick layers can be monitored [3].

The a-Si layers were prepared as follows. The Si single-crystal substrates were contacted to an LN$_2$-cooled stage during implantation. Uniform amorphous layers of various thicknesses were prepared by multiple MeV implants of [28]Si with overlapping damage profiles. The implantation schedules used to form layers of several different thicknesses are given in table 1. SPE kinetics measurements were conducted both in vacuum ($P < 5 \times 10^{-7}$ Torr) and in air. Fig. 1 shows the reflectivities measured at $\lambda = 1.15$ μm and $\lambda = 0.633$ μm during SPE growth of a 4.16 μm thick film heated to 625°C in vacuum. The $\lambda = 1.15$ μm trace exhibits uniformly spaced oscillations throughout the entire growth period, indicating that the velocity of the c/a interface is constant through the film. Additionally, aside from minor fluctuations, the amplitude of oscillations observed in this in situ interferometry measurement equals the value expected for an ideal film having perfectly flat and parallel interfaces. The excellent interference contrast throughout the growth also implies that competing

Table 1

Ion implantation conditions used to form thick a-Si layers. Implants were performed with the sample at 77 K. Thicknesses listed here were determined from TRR data. From Roth et al. [3]

a-Si thickness [a] [μm]	[28]Si energy [MeV]	dose [10^{15} cm^{-2}]
0.9	0.5	5
1.4	1.0	5
2.2	2.0	5
3.0	3.5	6
3.7	5.0	7
4.3	6.5	8

[a] A uniform amorphous layer of a particular thickness is obtained by using all of the implants up to and including the one listed for that thickness.

effects such as nucleation and growth of polycrystalline material or twin formation do not occur. The oscillation amplitude increases gradually with time during SPE due to reduced attenuation as the a-Si layer gets thinner. Due to the much stronger optical absorption in a-Si at $\lambda = 0.633$ μm, oscillations in the TRR data at this wavelength are only evident during the latter stages of growth. The temperature dependence of the SPE growth rate for 2.2 μm thick a-Si films is given in fig. 2. Fitting the data to an Arrhenius expression for the SPE rate $r = r_0 \exp(-E_a/kT)$ yields the value 2.70 ± 0.02 eV for the activation energy E_a. This is in excellent agreement with the 2.68 ± 0.05 eV activation energy found earlier for self-ion-implanted 300 nm films [2] and with the value 2.71 ± 0.05 eV for a-Si films formed by evaporation in ultrahigh vacuum [2]. To test whether the SPE rate in very thick a-Si layers is sensitive to the total amount of displacement damage caused by ion implan-
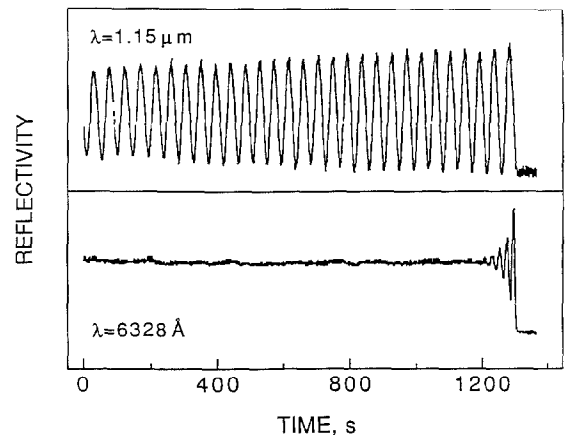

Fig. 1. Time-resolved reflectivity data at $\lambda = 1.15$ and $\lambda = 0.633$ μm for SPE growth of 4.16 μm thick, ion-implanted a-Si at 625°C in vacuum. From Roth et al. [3].
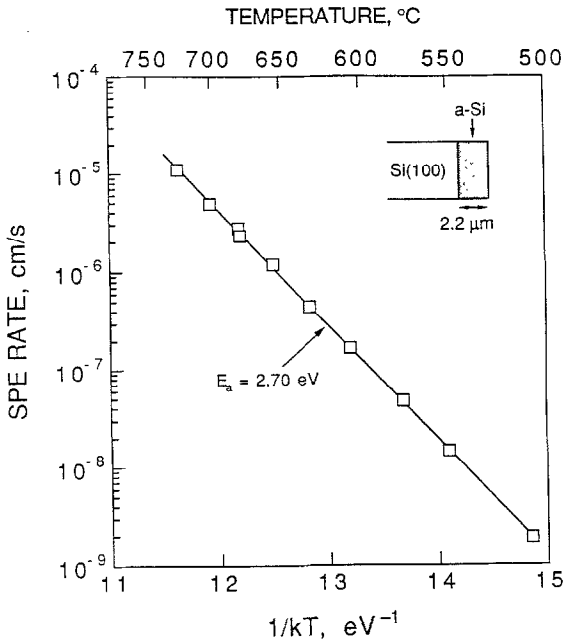
TEMPERATURE, °C

Fig. 2. Arrhenius plot showing the temperature dependence of the SPE rate in a 2.2 μm thick a-Si film formed by MeV ion-implantation. The solid line is a least-squares fit of the data to the expression $r = r_0 \exp(-E_a/kT)$. From Roth et al. [3].

tation, the rate was also measured in samples implanted at doses more than 1000 times above the threshold required to create an amorphous layer. The threshold dose for forming a thin, buried amorphous layer at 77 K using 1 MeV ^{28}Si irradiation is 2×10^{14} cm^{-2}. Previously amorphized films 2.2 μm thick were implanted with 1 MeV ^{28}Si ions at doses up to 2×10^{17} cm^2 in order to create an extra damage distribution peaked near the middle of the original amorphous layer. The SPE rate as a function of interface position was accurately measured, and no difference due to the extra implant was observed. It is interesting that the SPE rate does not change over this wide range of implant conditions, suggesting that the state of a-Si once formed is insensitive to additional ion bombardment.

The uniformity of the oscillation period in the TRR data in fig. 1 indicates that SPE occurs at a constant rate over distances greater than 4 μm when annealing is performed in vacuum. A marked deviation from this behavior is observed, however, when a-Si specimens are heated in normal room air. At depths approximately 1 μm from the surface the regrowth velocity is seen to decrease by as much as 40%. This effect has been correlated with the presence of water vapor in the annealing ambient and the growth of a surface oxide. The only impurities detected in the a-Si are hydrogen. These results indicate that atomic H is formed as a by-product of the oxidation of the a-Si during annealing

in the presence of water vapor [4] (Auger analysis showed that a thick ($\sim$ 5 nm) native oxide forms on a-Si during annealing in air). Once H is formed at the SiO$_2$/a-Si interface, it can diffuse rapidly [5] into the a-Si and attach to dangling bonds [6]. The solubility of H in c-Si is much lower than in a-Si due to the absence of defect sites, thus explaining why H is not seen in fully recrystallized layers.

The possibility that H affects the SPE rate is very intriguing since H is known to passivate dangling bonds in both deposited [6] and ion-implanted [7] a-Si films. Several different defect-based models involving dangling bonds [8], vacancies [9] and floating bonds [10] have been proposed for the mechanisms of SPE but no experimental data have been available to discriminate between the different defects. An understanding of the effect of H on the crystallization process should help contribute to the development of a microscopic model for SPE in a-Si.

3. Heat release, relaxation and defects

Our original experiments [11] on the formation of μm thick a-Si layers by MeV inert gas atoms produced enough material to measure the heat of crystallization, ΔH_{ac}, by differential scanning calorimetry (DSC). The heat of crystallization, 12.0 ± 0.7 kJ/mol, was used to estimate from free-energy consideration, the melting temperature of a-Si; a first-order phase transition. This estimate of the reduction, $\sim 250°$C, in melting temperature beneath the crystal melting temperature was confirmed by direct measurement [12] of the reduction, 225 ± 25 K. Some questions remained, however, concerning the state of the amorphous phase and the nature of the amorphous-to-crystal transition. The crystallization velocity was determined from the DSC net power signal. The definitive TRR [2] study of interface velocities gave values of velocity that were lower in magnitude and had a higher activation energy than those obtained from the DSC study. Second, the relative values of ΔH_{ac} for a-Ge and a-Si were surprisingly close: 11.5 and 12.0 kJ/mol, respectively. If ΔH_{ac} arises only from relief of bond angle distortions of the connected random network, ΔH_{ac} should scale with the force constants for the distortion, which are 15–20% higher in Si than Ge [11].

The most obvious difference between the a-Ge and a-Si data was a low-temperature heat release, clearly measured in Ge but not seen in Si. This release was mostly homogeneous in nature, and not primarily associated with interface motion. For a-Ge the homogeneous heat release was determined to be 6 kJ/mol over the range 400–600 K. In the case of a-Si, where higher temperatures made the base line curvature problems more severe, the net DSC signal below the crystalliza-

tion peak varied between endothermic and exothermic, indicating a much smaller homogeneous release. Nevertheless, annealing-induced relaxation effects on the optical properties such as the width of the Raman transverse optical band [13] or the infrared indices of refraction [14,15] have been observed in both a-Ge and a-Si. The situation has been clarified by the recent DSC measurements of Roorda et al. [16] of a low-temperature heat release from a-Si formed by Ar and Si implantation. They measured a homogeneous heat release of 3.7 ± 0.2 kJ/mol and an interfacial heat release $\Delta H_{ac} = 11.7 \pm 1.0$ kJ/mol. These important findings were confirmed [17] by using the 2.2 μm thick layers described in the previous section.

Fig. 3 shows DSC scans for as-implanted (lower) and samples that had been preannealed in a furnace at 525, 670 and 820 K, respectively. Two regimes are seen: at high temperature crystallization dominates, and over the entire 400 K lower-temperature region a fairly uniform release occurs. Samples that were preannealed show no heat release below the preannealing temperature, similar to the earlier observations in Ge. Since no motion of the a–c interface was observed by RBS after the 525 and 670 K anneals, the low-temperature signal corresponds to a one-time homogeneous heat release in the bulk of the a-Si. The kinetic parameters for crystalli-
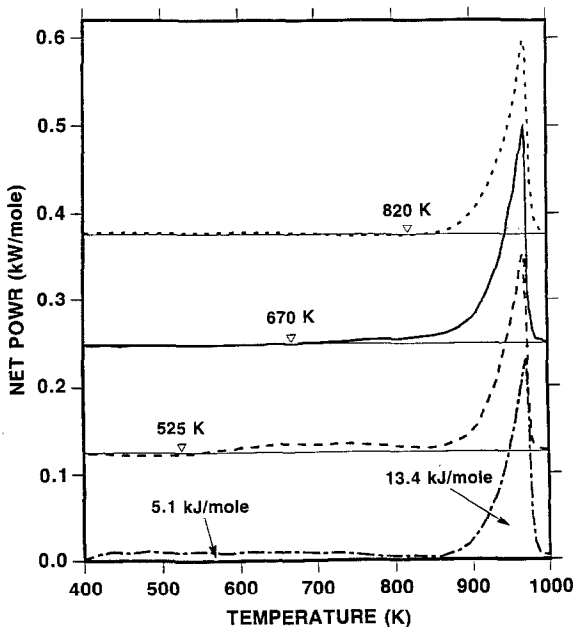

Fig. 3. DSC signals with base lines subtracted. The lower signal shows the as-implanted sample, the other three show samples that had been annealed in a furnace at 525, 670 and 820 K, respectively. The high-temperature part of the signal (crystallization) was fit to an exponential with an activation energy of 2.62 eV and was integrated to give an enthalpy of crystallization of 13.4 kJ/mol. From Donovan et al. [17].
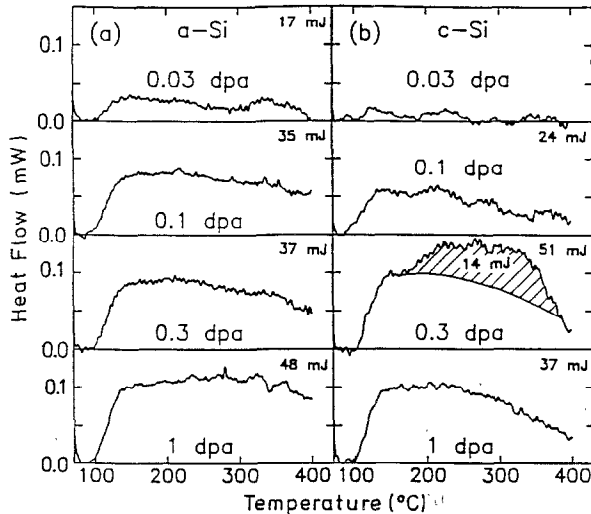
zation can be determined directly from an Arrhenius plot for the high-temperature DSC signal that gives crystallization velocity and has an activation enthalpy of 2.62 eV. This is in excellent agreement with the TRR measurements. By fitting an exponential with the appropriate activation enthalpy to the data down to the base line and integrating under this curve, the heat of crystallization, without any contribution from the homogeneous heat release, was determined. The average value from the measurements is 13.4 ± 0.5 kJ/mol. The average value of the remaining part, corresponding to the homogeneous heat release, is 5.1 ± 1.2 kJ/mol. The estimated error, taking into account all possible systematic errors, is ~ 6%. This gives as the new value of the heat of crystallization of a-Si: $\Delta H_{ac} = 13.4 \pm 0.7$ kJ/mol. This is ~ 10% higher than the earlier value, which was obtained by drawing a base line from the crystallized region to the onset of the peak and hence was an underestimate. That the new value of ΔH_{ac} for Si is higher than that for Ge is in better agreement with the relative values of the force constants for bond bending. It also explains why the earlier velocity data differed from the TRR data.

The observation of the low-temperature release in a scanning experiment, such as that of fig. 3, depends sensitively on the stability of the base line. It was therefore useful to perform isothermal experiments, since the base line is always a simple horizontal line (constant). A monotonically decreasing exothermal signal was observed in all cases [17,18]. This unambiguously confirms the existence of a low-temperature heat release. The data were fit with an exponential decay with typical delay times of 100 s. The fact that the low-temperature heat release was not observed in the earlier experiments was probably due to the inherent difficulties in background subtraction; the DSC technique was improved in the later measurements.

The question remains as to the physical mechanisms of the low-temperature release. In recent years there has been much discussion of the physical changes observed during annealing of a-Si without crystallization. This relaxation process had been interpreted in terms of changes in average bond angle distortion [13,14]. Our experiments [18–20] have resolved some of these issues. It was postulated that relaxation is primarily defect annealing. This postulate was checked by introducing defects by ion bombardment into annealed or relaxed a-Si, the samples being annealed at 500°C. Equivalent doses were also introduced into c-Si. The annealing characteristics, determined by calorimetry, of bombardment damage in relaxed a-Si and in c-Si were compared directly. Fig. 4 shows the low-temperature DSC traces of (a) well-relaxed a-Si and (b) c-Si, after irradiation with He$^+$ ions for a range of ion fluences. The curves for ion doses resulting in less than 0.03 displacements per atom (dpa) did not differ significantly from the

Fig. 4. Low-temperature DSC difference traces for (a) well-re-laxed a-Si and (b) c-Si, after bombardment with keV He$^+$ ions. The hatched area is discussed in the text. The values of the integrated heat release are shown. From Roorda et al. [18,20].

zero-signal base line and are not shown. The curves for 0.03 to 1 dpa a-Si (fig. 4a) deviate clearly from the base line, and show a heat release similar to that observed when as-implanted a-Si is ramp heated for the first time [16,17]. Saturation occurs between 0.03 and 0.1 dpa. Thus, bombardment with He$^+$ ions yielding 0.03 (or more) dpa in well-relaxed a-Si results in "de-relaxation" of the a-Si, i.e., the a-Si returns to the unrelaxed state which cannot be distinguished from as-implanted a-Si.

For c-Si (Fig. 4b), the curve for 0.03 dpa is not significantly different from the base line but the curve for 0.1 dpa indicates a heat release which is qualitatively similar to the signal from a-Si. This sample contains damage which has been identified, on the basis of RBS and TEM results, as a distribution of point defects and small point-defect clusters. After the DSC analysis to 400°C the damage has disappeared leaving a perfect crystal. It is concluded, therefore, that the heat release for the 0.1 dpa c-Si is due to annihilation of point defects and small point-defect clusters only. These point defects seem to anneal out continuously over a range of temperatures, as opposed to annealing kinetics domi-nated by only a few processes. Such annealing behavior implies a zoo of point defects in irradiated c-Si, with a large number of routes to annihilation. The area under the curve for 0.1 dpa c-Si corresponds to the total amount of heat released, this is 30% less than from 0.1 dpa a-Si. Combining the number of displaced atoms with the integrated heat release gives 0.56 eV per dis-placed atom. This may serve as an estimate of the stored energy per defect, but it is emphasized that the number of displaced atoms as determined by RBS is not

necessarily equal to the number of point defects. For 1 dpa the signal from c-Si resembles that from a-Si, but with somewhat reduced magnitude. In fact, this is the dose where the sample has just been made amorphous and the DSC signal is due to relaxation of this as-im-planted a-Si.

The curve for 0.3 dpa c-Si, which contains bands of extended defects and/or amorphous zones, differs from all other curves: a heat release can be seen which is larger than any other. Moreover, this curve is qualita-tively different because above 180°C an extra heat release begins (hatched area), which can be understood in terms of recrystallization of amorphous zones at anomalously low temperatures. The assumption is made that the heat release from 0.3 dpa c-Si is a linear superposition of annihilation of point defects (i.e., 0.56 eV/displaced atom) and heat release from crystalliza-tion and relaxation of amorphous zones (0.12–0.16 eV/atom [16,17]). The contribution from point defect annihilation should have the same onset and form as that from 0.1 dpa c-Si. The hatched area corresponds, therefore, to heat release from amorphous zones. From the measured heat release, the hatched area in fig. 4 would then correspond to $(8.2-6.2) \times 10^{17}$ atoms/cm^2 and the remaining area to 4.6×10^{17} displaced atoms/cm^2, thus giving a total number of $(1.3-1.1) \times 10^{18}$ displaced atoms/cm^2. This number is in good agreement with the channeling estimate of 1.3×10^{18} cm^{-2}. It is remarkable that the onset of epitaxial re-crystallization in the 0.3 dpa c-Si occurs at 180°C, but recrystallization of small amorphous zones at these low temperatures has been reported before [21]. One possi-ble reason for this phenomenon is that these small amorphous zones are embedded in a sea of defects which can enhance crystallization.

These collisional and defect ideas have been checked by bombarding relaxed a-Si with MeV C, Si and Ge ions [18,19] and examining the a-Si with Raman spec-troscopy. The transition from the relaxed to unrelaxed state occurs for ion doses on the order of 0.02 dpa irrespective of the mass of the projectile. Therefore it can be concluded that the phenomenon of de-relaxation by ion beams is due to the introduction of defects by nuclear collision. The similarity of the calorimetry data of fig. 4 strongly supports the contention that the zoos of defects introduced into a- and c-Si by ion bombard-ment are similar. Moreover, their annihilation proper-ties are very similar. These similarities seem to be con-firmed by the following observation.

A rough estimate of the defect densities involved in structural relaxation can be made by comparing the stored energy per displaced atom in c-Si determined from fig. 4b (0.56 eV) with the integrated heat release from 0.03 and 0.1 dpa a-Si (fig. 4a). Under the assump-tion that the average heat release from one annihilation event in a-Si is equal to that in c-Si, this yields defect

densities of 3.5 and 7.3 at.% in 0.03 and 0.1 dpa a-Si, respectively. It must be kept in mind that this analysis relies on a RBS and channeling measurement of the number of displaced atoms in 0.1 dpa c-Si which is not necessarily equal to the number of defects. Nevertheless, the agreement of this estimate of the defect density in a-Si with the Monte Carlo calculations is striking.

4. Density and defects

The density of a solid can give important clues regarding defect density. Moreover, in light of the previous discussion, it is interesting to measure the density in both the relaxed and unrelaxed configuration. The density of a-Si relative to the crystal, for example, has been a source of much debate. Early X-ray diffraction data indicated an amorphous density as much as 10% below [22] that of the crystal, although this was attributed to the presence of voids in the vapor-deposited films. Brodsky et al. [23] interpreted Rutherford-backscattering measurements in combination with surface profilometry to conclude that a-Si could be up to 1% denser than c-Si, although the measured density of their electron-beam-deposited a-Si films was 3% less dense than c-Si. Direct density measurements using weighing and interferometry of a-Ge deposited at the highest possible temperature indicated a density 1% higher than c-Ge [24]. Computer models of the structure of a-Si, assuming a continuous random network (CRN) without point defects, predict that the amorphous phase should be 3–4% more dense than the crystal [25]. Attempts to estimate the density of a-Si using molecular dynamics simulations have lead to results on either side of c-Si [26]. Recent experimental results on thin implanted layers indicate an a-Si density between 1.7 and 2.3% less than the crystal [27].

The availability of the high-energy Si ion beams has made it possible to produce thick, well characterized amorphous layers whose density can be accurately measured [28,29]. Alternating stripes of a-Si ($\sim$ 300 μm) and c-Si ($\sim$ 100 μm) were produced by MeV Si ion implantation through a steel mask into $\langle 100 \rangle$ Si. The relative density was then determined by measuring the physical step height at the lateral a–c-Si boundary. The implants were performed at a series of energies from 0.5 to 8.0 MeV with irradiation conditions chosen to ensure complete amorphization to the surface. All irradiations, except one, were performed with samples heat-sunk with vacuum grease to a copper block held at liquid-nitrogen temperature. The measured temperature rise during similar irradiations was less than 20°C. A single sample was irradiated at room temperature, again heat-sunk to the block, to check for density variations caused by the implant conditions. A wider range of a-Si thicknesses was obtained by partially recrystallizing the layers

at 500°C in a vacuum annealing furnace with a base pressure of $\sim 10^{-7}$ Torr. In addition, a section of each sample was thermally relaxed by annealing for one hour at 500°C.

The areal densities (at/cm^2) of the a-Si layers were measured by RBS in the channeling configuration using 3 MeV ^{4}He. Areal density can be converted into a film thickness using the density of a-Si ($\sim 4.9 \times 10^{22}$ at/cm^3). The maximum observable depth is limited by dechanneling in the a-Si to ~ 2.8 μm. The conversion of energy loss to areal density depends on the stopping powers for ^{4}He; however, two accepted sets of experimental measurements differ by up to 6% from each other [30,31]. Since this conversion represents a systematic error substantially larger than any other errors in the measurement, results are presented using both sets of stopping powers. Amorphous thicknesses between ~ 2.8 μm and 3.4 μm were estimated by measuring the thickness after partial solid-phase epitaxy. The resulting annealed thickness was extrapolated back to obtain the original as-implanted thickness using the measured epitaxial crystallization kinetics [3]. Surface profiles of the alternating a-Si and c-Si lines were obtained for each sample using a Tencor Instruments Alpha-step 200 surface profilometer calibrated with an NIST traceable standard. Typical scans are shown in fig. 5a for an as-implanted layer of 2.1 μm and for other thicknesses obtained by SPE from this implant set. Fig. 5b shows the corresponding RBS channeling spectra for these samples. Prior to determining the density difference, a small correction must be applied to the measured step heights to account for the Si implanted and sputtered [32] during amorphization. For example, at
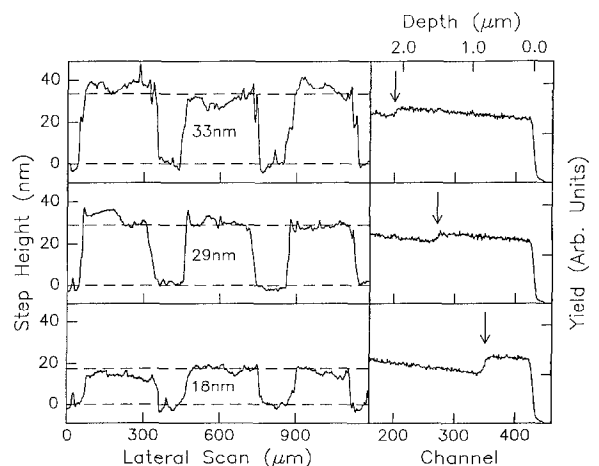

Fig. 5. (a) Surface profilometer traces of 2.1, 1.5 and 0.8 μm thick a-Si layers produced by 0.5–2.0 MeV series implants and epitaxial recrystallization. (b) Channeling spectra of samples shown in (a). The a-Si thicknesses are indicated. From Custer et al. [29].

2.0 MeV the implanted material adds 1.0 nm while sputtering removes 0.15 nm, giving a net addition of 0.85 nm.

Converting the measured step heights into a density difference requires knowledge of how the volume change is accommodated. The volume increase from c-Si to a-Si can be accommodated in several ways; a-Si can be formed with built-in stress, the substrate can plastically deform, or the a-Si can plastically deform. Measurements on laterally continuous 1 μm a-Si layers demonstrate that the volume change is primarily accommodated by a vertical strain with the in-plane strain less than 1% of the total strain [33]. This indicates that a-Si deforms plastically during formation by ion implantation. In the constrained geometry of these experiments, plastic deformation of the a-Si occurs for implants below 5 MeV and the entire volume change is exhibited as a vertical expansion. Below 5 MeV, little deformation of the surrounding c-Si is observed. However, for the higher-energy implants, plastic deformation of the constraining c-Si can be readily observed.

Step height data from samples implanted up to 5 MeV are shown in fig. 6 versus the areal densities of the a-Si layers. As-implanted samples are shown by the open circles and partially recrystallized or relaxed samples by filled squares. Within the error bars, step heights
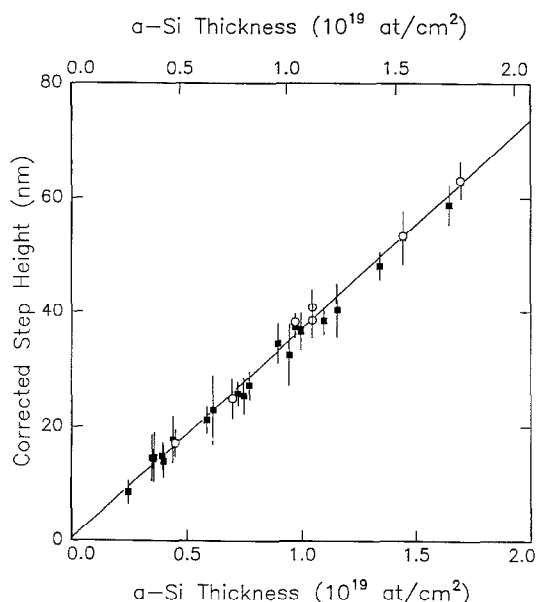

Fig. 6. Corrected step height vs a-Si areal density for as-implanted samples (open circles) and annealed samples (filled squares) of all implant series from 0.5 to 5.0 MeV. The areal density was obtained using the stopping powers of either Ziegler [30] (bottom axis) or Santry and Werner [31] (top axis). The solid line shows the step height expected for a 1.73% density difference (Santry and Werner values). From Custer et al. [29].

measured for the room temperature implanted sample were identical to those measured on samples implanted at liquid-nitrogen temperature. In addition, no differences in density could be detected between unrelaxed, relaxed or regrown samples, nor between samples implanted at any energy up to 5 MeV. Converting the areal density (using stopping powers of ref. [31]) to a-Si thickness and fitting a least-square line (with consideration for the individual error bars) through all the data yields a density difference of (1.74 ± 0.06)%. Fitting only as-implanted (unrelaxed) samples, the density difference is (1.79 ± 0.13)% while for annealed (i.e., relaxed) samples it is (1.70 ± 0.07)%. Considering the relative and absolute uncertainties in the stopping power measurements, an average value of (1.8 ± 0.1)% is the best estimate of the difference between the a-Si and c-Si densities. Very recent wafer-curvature experiments [34] have shown that the a-Si densifies by 0.15% on annealing to 500°C.

These measurements therefore raise several intriguing issues. First, the sign of the density difference is the opposite of that predicted by fully coordinated CRN models [25]. This means that defects have to be introduced into the CRN to make a realistic model. Moreover, the density change on annealing is very small even though the relaxation or annealing process discussed in the previous section consists of the annihilation of large defect populations. These results should give important clues as to the fundamental nature of the defects.

5. Diffusion and defects

The study of diffusion mechanisms can be a critical probe of the atomic structure of a solid. Little is known about diffusion in a-Si. In our earlier studies [35,36] it was established that Cu, Ag and Au are fast diffusers in a-Si and moreover there was a remarkable correlation between diffusion in a- and c-Si. This correlation is shown in fig. 7 for Au [36]. Why there is such a correlation in absolute magnitude and activation energy is an intriguing puzzle. It can be generally stated [37] however, that the fast diffusers in c-Si, with interstitial components, are fast diffusers in a-Si and that the slow, substitutional, diffusers in c-Si exhibit similar behavior in a-Si. The solubility of fast diffusing species in a-Si was also found to be at least six orders of magnitude greater than their solubility in c-Si.

Recent experiments by us [38,39] throw light on the diffusion mechanisms. A systematic study [38] of impurities implanted in thick a-Si layers has revealed more diffusing species (Zn, Pd and Pt), as shown in fig. 8. It should be noted that Cu and Pd are pure interstitial diffusers in c-Si while the remaining species are hybrid diffusers, i.e., they diffuse interstitially but exchange with substitutional sites. As was discussed in the previ-
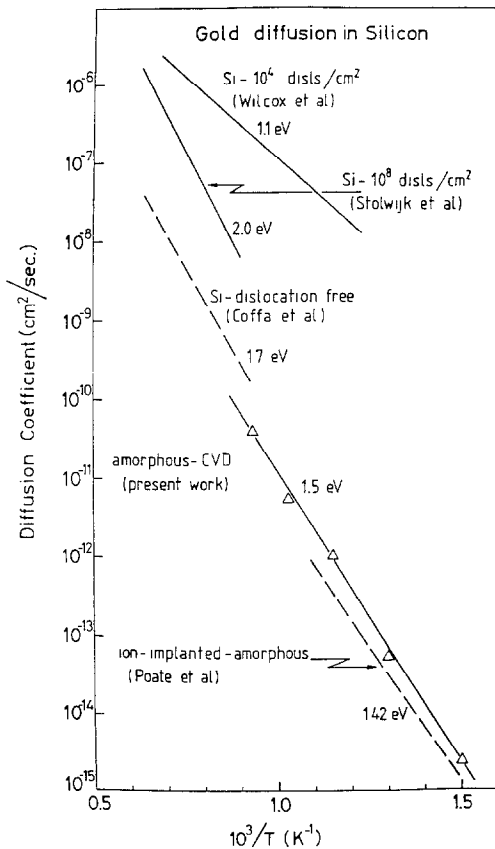
Fig. 7. Diffusion coefficients vs temperature for Au implanted a-Si and ion-implanted a-Si. For comparison the diffusion coefficients in dislocation-free single-crystal Si and dislocated Si are shown. From Calcagno et al. [36].
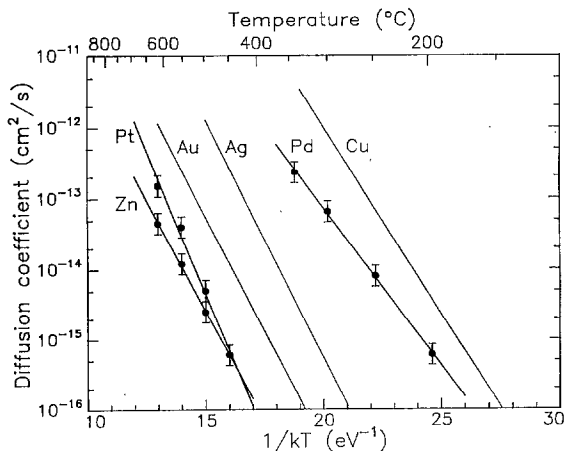

Fig. 8. Diffusion coefficients of implanted metallic impurities in a-Si. Diffusion was measured by RBS techniques in thick as-implanted a-Si. From Coffa et al. [38].

ous sections, a-Si contains a high density of defects whose population can be reduced by annealing. The effect of these defects on diffusion is dramatically demonstrated in the following experiment [39]. It is known that the fast diffusing impurities such as Cu can be trapped or gettered at defects in c-Si. Analogous behavior is shown here for Cu in a-Si.

Amorphous Si layers, 2.2 μm thick, were prepared in the as-implanted and also in the relaxed 500°C annealed state. The samples were then implanted with 200 keV Cu ions to a dose of 5.5×10^{15} ions/cm^2. The diffusion of Cu in all samples was then studied following thermal treatment at various temperatures ranging from 150 to 270°C, for times between 20 min and 104 h (the terminology "annealing" refers to heating of the a-Si at 500°C for 1 h and "thermal treatment" to the subsequent heating used to induce the Cu diffusion). The Cu concentration profiles were measured using 4 MeV ^{4}He^{2+} backscattering with a scattering angle of 125°. Fig. 9 shows Cu RBS spectra of the unannealed and annealed samples, before and after thermal treatment for 4 h at 221°C. As can be seen, the as-implanted Cu profile peaks at ~ 100 nm below the surface. The peak Cu concentration amounts to 0.7 at.%. After thermal treatment on the unannealed sample, significant
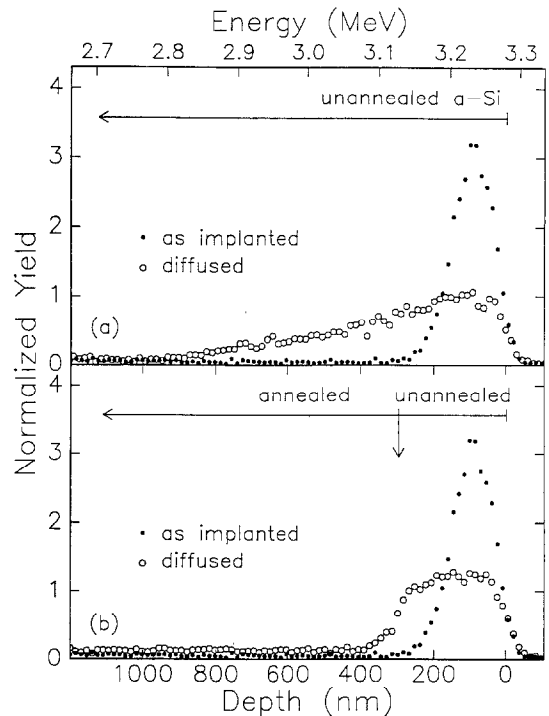

Fig. 9. Backscattering spectra of two types of Cu implanted a-Si samples before and after thermal treatment at 221°C for 4 h: (a) unannealed a-Si, (b) double-layer of annealed and unannealed a-Si. From Polman et al. [39].

in-diffusion of Cu is observed (fig. 9a) with diffusion distances in agreement with parameters previously measured [35].

An entirely different diffusion behavior is observed in the annealed sample (fig. 9b). A uniform Cu concentration is observed in an approximately 300 nm thick surface layer, and a low-concentration Cu tail is observed in the deeper-lying annealed layer. The interface between the two concentration regions coincides with the end of range of the Cu implant, which has returned the 300 nm thick surface region to the as-implanted, unannealed state. The diffused Cu concentration in the 300 nm surface layer in fig. 9b is higher than in the corresponding region in fig. 9a. This indicates that during diffusion, Cu is partially reflected at the interface between annealed and unannealed a-Si. Such behavior is characteristic for solute partitioning at a phase boundary. The ratio between the Cu levels in the two a-Si phases can then be interpreted as a partition coefficient (k), and amounts to $k = 9 \pm 1$ in this case. A diffusion experiment has also been performed in a similar structure as in fig. 9b produced by half the Cu fluence, giving a value of $k = 10 \pm 2$. The discontinuity in the Cu profile is quite abrupt. This abruptness can be understood from the fact that at the end of range of the damage (dpa) profile of the Cu implant is a rapidly decreasing function of depth, resulting in a sharp phase boundary between unannealed and annealed a-Si. The Cu tail in fig. 9b extends deeper than that in fig. 9a, indicating that the diffusion coefficient in annealed a-Si is higher than in unannealed a-Si.

Additional studies were performed to determine diffusion and partition coefficients over a wide temperature range. Fig. 10 shows a Cu concentration profile in the annealed/unannealed layer structure after thermal treatment at 170°C for 20.5 h. It also shows results of numerical calculations of the Cu profile taking into account total reflection at the surface and partitioning at the annealed/unannealed interface. The line represents a best fit, obtained using $k = 7$ and a ratio of 2 between the diffusion coefficients in annealed and unannealed a-Si. In additional experiments it was found that, within the error bars, the partition coefficient was not very sensitive to the diffusion time and temperature in the temperature range between 150 and 270°C; an average of $k = 8.2 \pm 1.3$ was obtained. Also, it was found that the partition coefficient is smaller for samples in which the a-Si is annealed at a lower temperature, i.e., more defects in the starting material.

Fig. 11 summarizes the measured Cu diffusion coefficients in annealed a-Si in the temperature range 150–270°C in an Arrhenius fashion. The data from our earlier study on diffusion in unannealed a-Si are also shown [35]. These data are in agreement with coefficients found for the unannealed layer in the simulations described above. As can be seen, in the temperature
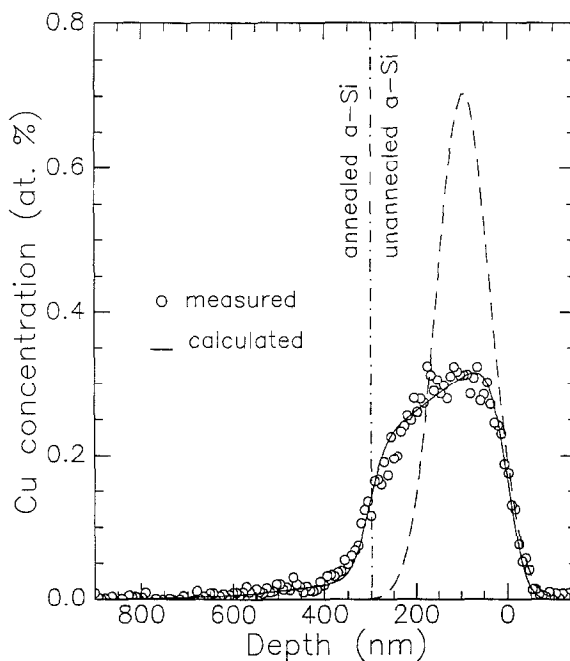

Fig. 10. Cu concentration as a function of depth in an unannealed/annealed double-layer structure after thermal treatment at 170°C for 20.5 h (circles). The dotted line is the as-implanted profile, the drawn line is a fit using numerical simulation of diffusion and solute partitioning. From Polman et al. [39].

range studied, the diffusion rate in annealed a-Si is a factor 2–5 higher than in unannealed a-Si. It should be pointed out that this behavior is opposite to that seen in the annealing of metallic glasses where the diffusivity decreases with annealing [40]. However, the defect annealing process in a-Si would appear to be quite different from that of a glass. The diffusion activation energy (E) in annealed a-Si is not significantly different than in unannealed a-Si ($E = 1.39 \pm 0.15$ eV vs $E = 1.25 \pm 0.04$ eV, respectively).

These Cu data show quite strikingly the role which defects can play in the a-Si structure. To first order, if it is assumed that Cu concentrations are correlated with defect concentrations, the data would imply that the defect concentration in the annealed material is one order of magnitude lower than that in the as-implanted, unannealed material. However, even in the annealed a-Si the Cu concentration is relatively high. The correlation of Cu concentration or solubility with defect concentration is plausible and leads to an interesting observation. The flat-topped Cu profile would indicate that the defects introduced by the Cu implantation are saturating over a distance of some 300 nm from the surface. Moreover, these defects influence the diffusion rate (fig. 11). Assuming that Cu is an interstitial diffuser in a-Si and is trapped at defect sites, then the diffusion
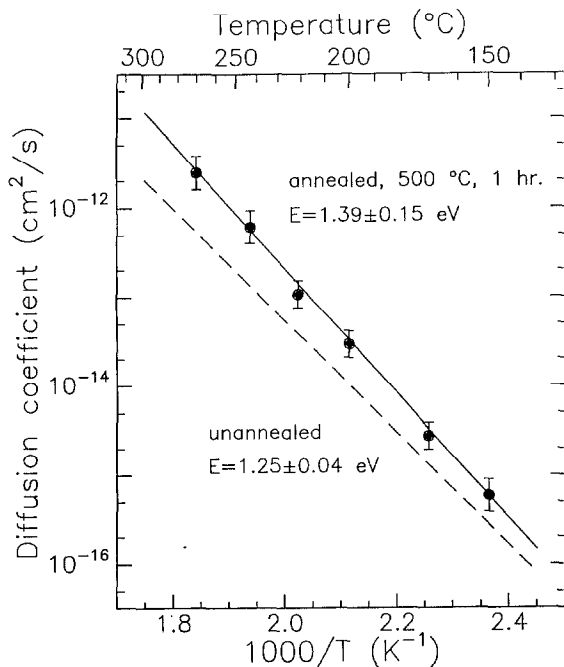
Fig. 11. Cu diffusion coefficients in a-Si annealed at 500°C for 1 h (circles). The drawn line is an Arrhenius fit to the data. Data from our earlier study [35] for unannealed a-Si are also indicated (dashed line). From Polman et al. [39].

coefficient will increase for lower defect concentrations, as is observed. Experiments are in progress to correlate the diffusion of some of the other species shown in fig. 8 with defect concentrations.

6. Conclusions

The experiments described here have solved some old puzzles and raised more questions regarding a-Si. The role of defects is seen to be crucial. Relaxation has been identified as a defect annealing process but even in the well-relaxed state the defect population is high. The diffusion of impurities is strongly influenced by defects and the fast diffusers such as Cu are remarkably sensitive markers of these defects. One message that comes through strongly from these data is that many of the defect production, annealing processes, impurity diffusion and solubility phenomena in a-Si can be thought of in terms of c-Si with a high defect population. The atomistic nature of these defects, however, has not been identified.

References

[1] J.M. Poate, in: Amorphous Si and Related Materials, vols. A and B, ed. A. Fritsche (World Scientific, New Jersey, 1989) p. 149.
[2] G.L. Olson and J.A. Roth, Mater. Sci. Rep. 3 (1988) 1.
[3] J.A. Roth, G.L. Olson, D.C. Jacobson and J.M. Poate, Appl. Phys. Lett. 57 (1990) 1340.
[4] A.G. Revesz, J. Electrochem. Soc. 126 (1979) 122.
[5] D.E. Carlson and C.W. Magee, Appl. Phys. Lett. 33 (1978) 82.
[6] P.G. LeComber, A. Madan and W.E. Spear, J. Non-Cryst. Solids 11 (1972) 219.
[7] H.J. Stein and P.S. Peercy, Appl. Phys. Lett. 34 (1979) 604.
[8] F. Spaepen and D. Turnbull, in; Laser-Solid Interactions and Laser Processing, eds. S.D. Ferris, H.J. Leamy and J.M. Poate (AIP Press, New York, 1978) p. 73.
[9] L. Csepregi, R.P. Kullen, J.W. Mayer and T.W. Sigmon, Solid State Commun. 21 (1977) 1019.
[10] S.T. Pantelides, Mater. Res. Soc. Symp. Proc. 100 (1988) 387.
[11] E.P. Donovan, F. Spaepen, D. Turnbull, J.M. Poate and D.C. Jacobson, J. Appl. Phys. 57 (1985) 1795.
[12] M.O. Thompson, G.J. Galvin, J.W. Mayer, P.S. Peercy, J.M. Poate, D.C. Jacobson, A.G. Cullis and N.G. Chew, Phys. Rev. Lett. 52 (1984) 2360; and unpublished data.
[13] W.C. Sinke, S. Roorda and F. Saris, J. Mater. Res. 3 (1988) 1202.
[14] G.K. Hubler, E.P. Donovan, K.W. Wang and W.G. Spitzer, Proc. SPIE 350 (1985) 222.
[15] E.P. Donovan, G.K. Hubler and C.N. Wadell, Nucl. Instr. and Meth. B19 (1987) 590.
[16] S. Roorda, S. Doorn, W.C. Sinke, P.M.L.O. Scholte and E. van Loenen, Phys. Rev. Lett. 62 (1989) 1880.
[17] E.P. Donovan, F. Spaepen, J.M. Poate and D.C. Jacobson, Appl. Phys. Lett. 55 (1989) 1516; and unpublished data.
[18] S. Roorda, Ph.D. Thesis (University of Utrecht and FOM-Instituut, Amsterdam, 1990).
[19] S. Roorda, J.M. Poate, D.C. Jacobson, S. Dierker, B.S. Dennis and W.C. Sinke, Appl. Phys. Lett. 56 (1990) 2097.
[20] S. Roorda, J.M. Poate, D.C. Jacobson, D.J. Eaglesham, B.D. Dennis, S. Dierker, W.C. Sinke and F. Spaepen, Solid State Commun. 75 (1990) 197.
[21] M.O. Ruault, J. Chaumont and H. Bernas, Nucl. Instr. and Meth. 209/210 (1983) 351.
[22] S.C. Moss and J.F. Graczyk, Phys. Rev. Lett. 23 (1969) 1167.
[23] M.H. Brodsky, D. Kaplan and J.F. Ziegler, Appl. Phys. Lett. 21 (1972) 305.
[24] T.M. Donovan, E.J. Ashley and W.E. Spicer, Phys. Lett. 32A (1970) 85.
[25] F. Wooten and D. Weaire, Solid State Phys. 40 (1987) 1.
[26] W.D. Luedtke and U. Landman, Phys. Rev. B40 (1989) 1164.
[27] W.G. Spitzer, G.K. Hubler and T.A. Kennedy, Nucl. Instr. and Meth. 209/210 (1983) 309.
[28] J.S. Custer, Ph.D. Thesis (Cornell University, Ithaca, NY, 1990).
[29] J.S. Custer, M.O. Thompson, D.C. Jacobson, J.M. Poate, S. Roorda, W.C. Sinke and F. Spaepen, Appl. Phys. Lett, in press.
[30] J. F. Ziegler, He Stopping Powers and Ranges in all Elemental Matter (Pergamon, New York, 1978).
[31] D.C. Santry and R.D. Werner, Nucl. Instr. and Meth. 159 (1979) 523.

[32] P. Sigmund, Phys. Rev. 184 (1969) 383.
[33] C.A. Volkert, Mater. Res. Soc. Symp. Proc. 157 (1990) 635.
[34] C.A. Volkert, unpublished data.
[35] J.M. Poate, D.C. Jacobson, J.S. Williams, E.G. Elliman and D.O. Boerma, Nucl. Instr. and Meth. B19/20 (1987) 480.
[36] L. Calcagno, S.U. Campisano and S. Coffa, J. Appl. Phys. 66 (1989) 1874.
[37] J.M. Poate, D.C. Jacobson, F. Priolo and M.O. Thompson, Mater. Res. Soc. Symp. Proc. 128 (1989) 533.
[38] S. Coffa, D.C. Jacboson, J.M. Poate, W. Frank and W. Gustin, to be published.
[39] A. Polman, S. Coffa, D.C. Jacobson, J.M. Poate, S. Roorda and W. Sinke, Appl. Phys Lett. 57 (1990) 1230.
[40] H.S. Chen, L.C. Kimerling, J.M. Poate and W.L. Brown, Appl. Phys. Lett 32 (1978) 461.